OPEN ACCESS
IOP Publishing
Classical and Quantum Gravity
Class. Quantum Grav. **40** (2023) 245006 (11pp) https://doi.org/10.1088/1361-6382/ad0923

Temperature dependence of the thermal conductivity of hydroxide catalysis bonds between silicon substrates

Mariela Masso Reid[1,*], Karen Haughian[1], Alan V Cumming[1], James Faller[1,2,†], Giles Hammond[1], James Hough[1], Anna-Maria van Veggel[1] and Sheila Rowan[1]

[1] SUPA, Institute for Gravitational Research, School of Physics and Astronomy, University of Glasgow, Glasgow, G12 8QQ, United Kingdom
[2] JILA, National Institute of Standards and Technology and University of Colorado, Boulder, CO 80309-0440, United States of America

E-mail: Mariela.MassoReid@glasgow.ac.uk

Received 18 July 2023; revised 17 October 2023
Accepted for publication 2 November 2023
Published 17 November 2023

Abstract

Future generations of gravitational wave detectors plan to use cryogenics in order to further reduce thermal noise associated with the mirror test masses and their suspensions. It is important that the thermal conductivity of candidate materials for these mirror suspension systems, and any additional thermal resistance associated with the required bonding/jointing, is characterised. Results are presented here for composite single-crystal silicon substrates, with multiple hydroxide catalysis bonds present, in order to assess the thermal conductivity of the bond layers. An average bond thickness of 460 nm is observed within the oxide-bond-oxide interfaces, with a calculated thermal conductivity rising from $0.013 \rightarrow 0.087\ \mathrm{Wm^{-1}K^{-1}}$ across a temperature range of $9 \rightarrow 300$ K. This confirms that the thermal conductance through hydroxide catalysis bonds, with geometries being considered for third generation gravitational wave detectors operating at 20 K or 125 K, would have a negligible impact on the required heat extraction for cryogenic operation. Therefore, the use of hydroxide catalysis bonding, as successfully demonstrated within room temperature gravitational

† Deceased.
* Author to whom any correspondence should be addressed.

wave detectors, remains an attractive solution for building future cryogenic instruments with reduced thermal noise and enhanced astrophysical reach.

Keywords: thermal conductivity, gravitational waves, hydroxide catalysis, bonding, temperature dependance, silicon

(Some figures may appear in colour only in the online journal)

1. Introduction

There have been 90 binary black hole and neutron star mergers observed in the first three observing periods of the advanced (second generation) interferometric gravitational wave detectors [1–3]. These signals were observed by Advanced LIGO [4, 5] and Advanced Virgo [6], which both operate at room temperature and employ monolithic silica test mass suspensions, as pioneered in the GEO600 detector [7, 8]. The monolithic silica suspensions are constructed using hydroxide catalysis bonding, which was developed and patented by Gwo [9–11] for assembling fused silica telescope components for Gravity Probe B [12]. This bonding technique played a critical role in reaching the detector sensitivities required to directly detect gravitational wave signals, due its favourable Brownian thermal noise performance [13, 14]. Brownian thermal noise can set an important limit on the sensitivity of gravitational wave detectors by causing thermally-driven displacements of the surface of the mirrors [15]. In order to further reduce thermal noise, future observatories propose operating at cryogenic temperatures ($\sim$20 K [16] and $\sim$125 K [17, 18]). Fused silica has a broad dissipation peak centred on 30 $\rightarrow$ 40 K [19–22] making it an unsuitable material for cryogenics, and thus the two materials of choice are silicon and sapphire. Silicon has typically been the preferred material due to beneficial thermomechanical properties, particularly the zero values of the linear coefficient of expansion, α, at $\sim$18 K and $\sim$124 K leading to the removal of thermoelastic thermal noise at these two temperatures [23]. These temperatures would also be relevant for minimising thermal lensing, which scales as α/κ (κ is the thermal conductivity) [23].

A previous study of bond thermal conductance was carried out on a hydroxide catalysis bonded sapphire sample with a single bond interface over a temperature range of 10 $\rightarrow$ 40 K [24]. It demonstrated excellent thermal conductance through the jointed substrates [24]. To successfully create a bond between silicon substrates, the silicon surfaces must first be oxidised. The presence of the two surface oxide layers required, along with the bond itself, leads to a thicker joint being created between silicon, impacting the final thermal conductivity, as opposed to the previously investigated sapphire. Another study was later carried out on a bonded oxidised silicon sample with one bond interface over a temperature range of 100 $\rightarrow$ 300 K [25]. It showed that the thermal conductivity through the sample was reduced by less than 20% from the bulk conductivity value due to the presence of the bond. However, the study was unable to accurately extract a bond thermal conductivity from the data. The results presented here are for three oxidised silicon samples created with multiple bonds to amplify the effects. The bond thicknesses are all characterized to allow the thermal conductivity of the bond material to be calculated directly. This investigation was carried out over a large temperature range, spanning 9 $\rightarrow$ 300 K.

2. Hydroxide catalysis bond formation between silicon substrates

For successful bonding of silicon, to avoid hydrogen production, a layer of silicon dioxide has to be formed on the surface and thus the chemistry is described as being between two silicon

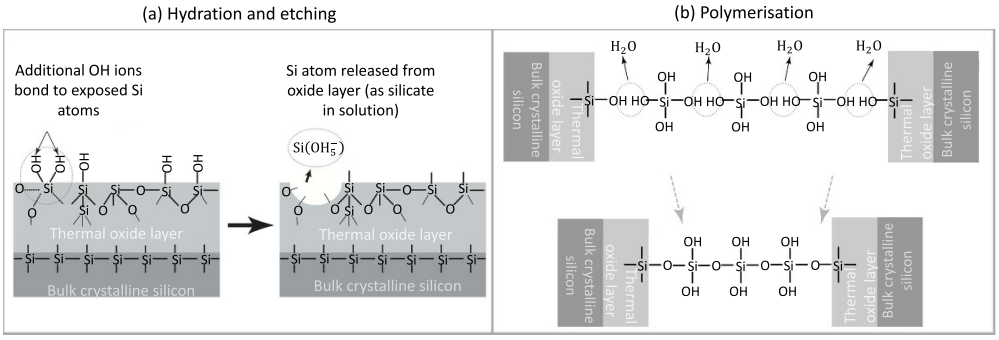

Figure 1. Illustration of (a) the hydrated silicon dioxide surface being etched in the presence of OH^- ions, and (b) the dehydration and polymerisation process that produces siloxane chains responsible for the chemical bonding process under investigation.

dioxide surfaces. The hydroxide catalysis bonding procedure is described in detail by several authors [26–28]. The process involves a hydroxide solution, which can contain silicate (e.g. sodium silicate, Na_2SiO_3), placed between the surfaces to be bonded. As shown in figure 1, OH^- ions occupy open bonds on the material's surface when hydrated. The presence of additional OH^- ions can create additional bonds to exposed silicon atoms, which can weaken and liberate molecules from the surface in the form of $Si(OH)_5^-$ [29]. When the pH of the solution is below 11 [29] the silicon ions dissociate to form $Si(OH)_4$ and OH^- such that,

$$Si(OH)_5^- \rightleftharpoons Si(OH)_4 + OH^-. \tag{1}$$

Initially the release of OH^- ions allows the etching to continue. However, as a monomer, $Si(OH)_4$ likes to form polymer arrangements (siloxane chains), causing the bonding solution to 'set'. The remaining H_2O within the bonding solution will evaporate and/or will be absorbed into the bulk material, allowing the bond to strengthen over time. Curing times are expected to be similar to bulk silica samples, with significant strength after approximately one week, due to nominally identical surface chemistry [9, 10, 30].

3. Sample fabrication

To enhance the contribution of the thermal resistance associated with the bonds, samples were fabricated with multiple bonds in series. The samples were fabricated between a pair of silicon blocks with cross sectional area 5×5 mm and 20 mm in length. Two samples (samples 1 and 2) were bonded with nine thin sections of thickness 550 μm (10 bonds), diced from a silicon wafer. A third sample (Sample 3) was also fabricated using 4 of the silicon blocks (3 bonds). Both sample configurations are shown in figure 2. In addition, 2 longer silicon block samples of $5 \times 5 \times 40$ mm were obtained and used as reference sample.

The silicon blocks were diced from an ingot (supplied by Prolog Semicor Ltd Kiev, Ukraine) with $<100>$ crystallographic orientation along their length, with both end faces polished to a nominal peak-to-valley flatness of $\lambda/10$ where $\lambda = 633$ nm. The silicon ingot was boron doped $(<0.01\%)$, grown using the Czochralski process, with stated resistivities of the ingot faces from the manufacturer as 2.17 Ωcm (bottom) and 2.47 Ωcm (top). The oxygen concentration was specified to be 5.3×10^{17} atoms cm^{-3} (top) and 5.0×10^{17} atoms cm^{-3} (bottom), with carbon concentration stated as 2.8×10^{16} atoms cm^{-3} (top) and 3.6×10^{16} atoms cm^{-3} (bottom). The fabricated blocks were measured with a four-point probe and found to have

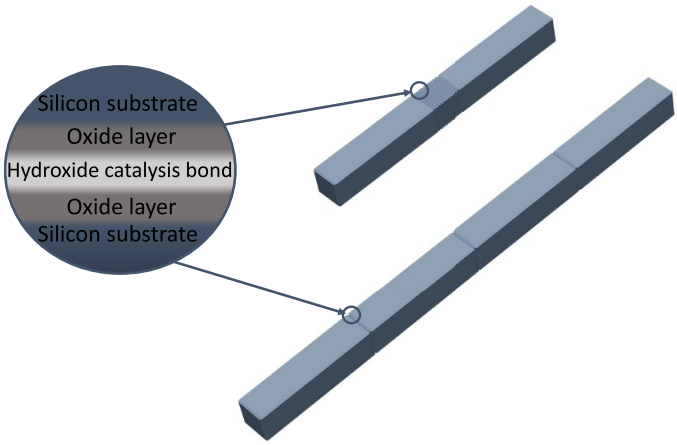

Figure 2. Sample fabrication detailing the layers needed for each bond as well as the two different types of samples used to achieve the results presented. Sample on the top left (smaller in size) represents samples 1 and 2 (composed of 10 bonds, located on the centre of the sample between nine, 550 5 × 5 mm, thin wafers. Sample on the bottom right represents Sample 3 (3 bonds, 1 between each 20 mm substrate).

resistivities around 3 Ωcm. The properties of the silicon wafer are not known except for the resistivity which was measured by the author to be 10 Ωcm. The flatness of each side of the blocks was measured before and after oxidation using a Zygo GPI XP/D interferometer at 633 nm. The silicon blocks and wafer were oxidised at 1000 °C for 4 h in a furnace, to grow an oxide layer of approximately 200 nm. The thermal oxidation process is described by Deal and Grove [31]. The oxide thicknesses were measured before bonding by ellipsometry and found to be in the range 100–700 nm, with the large variation possibly arising from differences in the thermal treatment conditions between samples e.g. due to the differing position in the furnace. The silicon wafer was diced using a DAD3230 automated dicing saw and the edges of the blocks were chamfered using custom metal tooling that held the sample at a 45° angle against a diamond sheet, to match the chamfered edges on the silicon blocks.

After characterising the heat flow through the samples, the thickness of the bonds were directly measured using an Hitachi TM-1000 tabletop scanning electron microscope. In order to image the substrate, oxide and bond layers, two of the samples (sample 1 and 2) were ground and then polished along their lengths to attempt to reveal a clear cross-section. The bonds and oxide layers that were measured were in the range of 320–1160 nm, due in most part to the oxide layer thickness variability. Sample 1, including all ten bonds, remained intact for the imaging with the bond and oxide layer average thickness found to be ≈775 nm. Sample 2 was damaged when polishing allowing only two bonds to be measured (average value of ≈505 nm) and so a range of thicknesses was used in section 5. The bond thickness was not directly measured for Sample 3, as this sample has been preserved for any follow-up studies of thermal conductivity. Since the component blocks of Sample 3 were found to have an oxide layer thickness of ≈130 nm, and since the previously measured bond thickness between flat silica substrates is ≈61 nm [32], the average bond thickness used for calculating the thermal conductivity was taken as ≈321 nm.

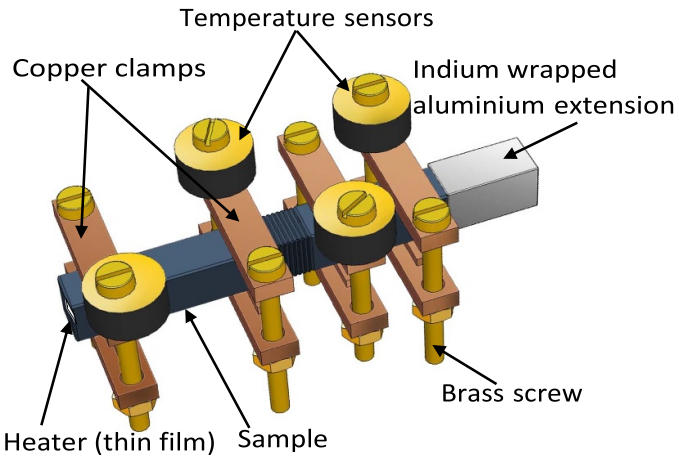

Figure 3. Schematic diagram detailing temperature sensor positioning and attachment for the bonded silicon samples (samples 1 and 2).

4. Thermal conductivity measurement

The *absolute steady state method* [33, 34] was used to measure the thermal conductivity of the composite silicon samples, by applying a constant heat flow through one end while holding the other end at a lower constant temperature. This temperature was maintained at a specified value by a thermal heat sink. The temperature of the heat sink was controlled by a heater on a feedback loop [33, 34]. Measurements were made under high vacuum ($\leqslant 10^{-6}$ mbar) in order to minimise gas convection and conduction [35] and performed in a cryostat to allow for measurements to be taken from 9 K $\rightarrow$ 300 K. The thermal conductivity, κ, can be calculated using the reciprocal of the temperature gradient, $\frac{\Delta T}{\Delta x}$, times the power, P, and divided by the cross sectional area, A, such that, ts, divided by the cross-sectional area, such that,

$$\kappa = \frac{P}{\Delta T}\frac{\Delta x}{A} = b\frac{\Delta x}{A}, \tag{2}$$

where b is the calculated gradient of a plot of power against temperature difference. The power is calculated from the measured voltage across and the calculated current through a resistive heater (Vishay thin film type resistor) placed on one end of each of the samples, used to provide a temperature gradient. To determine the current, the voltage is measured across a second resistor of known value, which is placed in series and external to the cryostat.

This allows the current in the circuit to be measured without introducing any uncertainty associated with the heater resistance value changing across the large temperature range.

The temperature sensors were clamped to the sample using aluminium, brass and copper elements due to their high thermal conductivities, to minimise the time for the temperature sensors to reach thermal equilibrium with the steady state temperature gradient of the sample. The Cernox CX-10XX-CU sensors employed are shown in figure 3. The temperature sensor locations and the full clamping set up are shown in figures 3 and 4.

The heat flow was assessed by measuring the temperature across four points on the sample, in addition to the aluminium block, which acts as a thermal sink. A thin layer of indium was soldered on the contact point between the clamp and sample to ensure good thermal contact. An aluminium extension (of length $\sim$1 cm) was bonded to the sample by cryo-compatible varnish, and provides increased separation between the mounted temperature sensors, by allowing

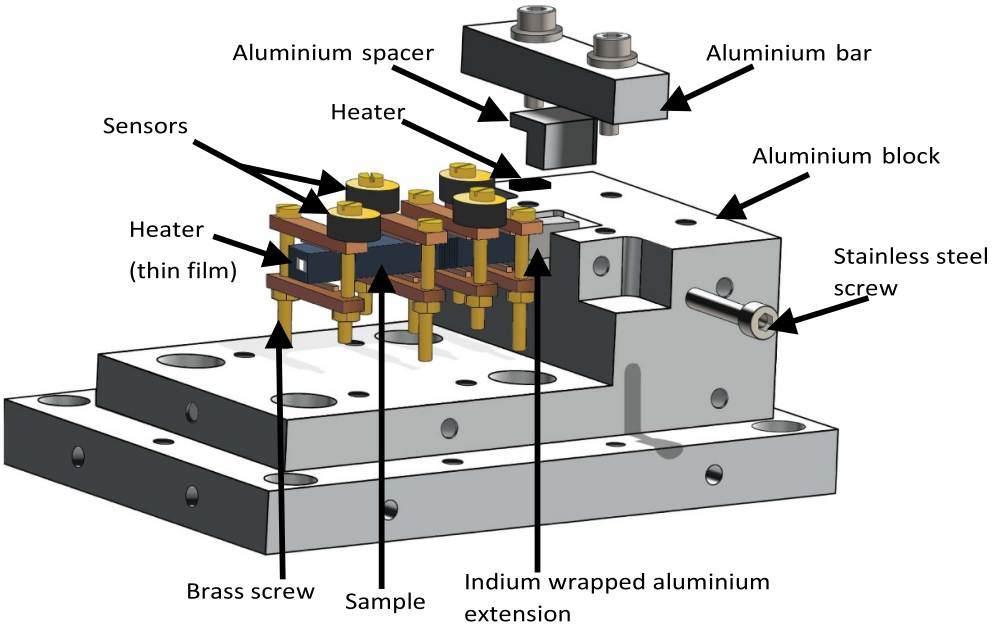

Figure 4. Schematic diagram showing complete the mounting structure used to assess the temperature gradients in the bonded silicon samples to investigate the thermal conductivities. A temperature sensor was also placed on the far wall of the aluminium block near the heater to provide sensing for the feedback loop. The labelled aluminium bar and stainless steel screw were used to apply a force on the aluminium spacer to ensure good thermal contact.

the majority of the silicon sample length to be outside of the clamping structure. An indium layer was then wrapped around the aluminium extension and end of the sample to improve the thermal contact between the sample and aluminium block, shown in figure 4. The bonded sample was held down by an aluminium bar which is pushed by screws from both the top and one side, in order to ensure good thermal contact between two surfaces. The cryostat was sealed and evacuated to 10^{-6} mbar before being cooled using liquid helium. Once cooled, the experiment was thermally stabilised and measurements were taken in increments of 1 K from 9 K to 30 K, then in increments of 2 K up to 100 K and an increased increment size up to 300 K.

5. Results

The thermal conductivity of the hydroxide catalysis bonds was assessed by measuring three different silicon samples, bonded as discussed, and comparing the temperature gradients and associated heat flows with respect to the measured thermal conductivity of reference silicon samples (average thermal conductivity measured for the 2 reference silicon samples).

The measured values for the thermal conductivity of silicon along with the total thermal conductivity of the hydroxide catalysis bonded samples are presented in figure 5. The thermal conductivity curve of the measured silicon peak reaches $\approx 1302 \pm 7\ \mathrm{Wm^{-1}K^{-1}}$ at around 40 K.

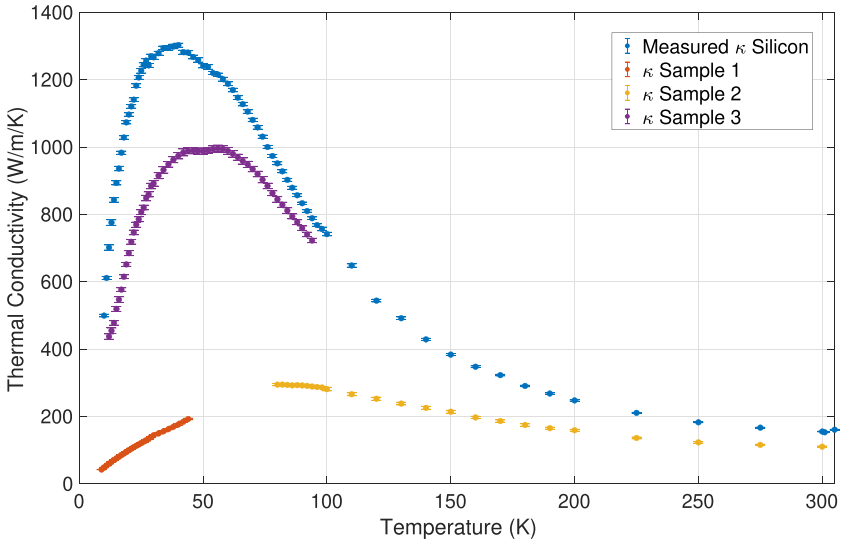

Figure 5. Measured overall thermal conductivity of samples 1, 2 and 3 compared to the measured thermal conductivity of silicon (average of two reference samples, as stated previously). The errors are calculated from a combination of systematic errors associated with the spacing of the sensors, the cross sectional area of the sample, and the statistical error from the measured power and temperature differences ($2\% \rightarrow 5\%$).

From the measured thermal conductivites, κ_{total} for samples 1, 2 and 3, and by considering the thermal resistances of the silicon elements and the bonds in series, the thermal conductivity of the bonds, κ_{bond} can be calculated as,

$$\kappa_{\text{bond}} = \frac{L_{\text{bond}}}{\frac{L_{\text{total}}}{\kappa_{\text{total}}} - \frac{L_{\text{silicon}}}{\kappa_{\text{silicon}}}}. \tag{3}$$

where κ_{silicon} is the average of the thermal conductivity measured on 2 separate reference samples, L_{bond} is the bond thickness, L_{silicon} is the silicon thickness and L_{total} is the separation of the temperature sensors on the sample. The thermal conductivity of the bond is then extracted for the measured temperature range, giving for example a thermal conductivity of $3.20 \pm 0.06 \times 10^{-2}$ Wm^{-1} K^{-1} at 20 K. The results are shown in figure 6.

An assumption was made where the thermal conductivity of the silicon blocks and the silicon wafers are to be nominally identical to each other, $\kappa_{\text{silicon}} \approx \kappa_{\text{wafer}}$. The electrical resistivity was measured for both the silicon blocks ($\approx 3\,\Omega$cm) and wafers ($\approx 10\,\Omega$cm) giving calculated boron densities of 1×10^{15} atoms cm^{-3} and 5×10^{15} atoms cm^{-3} respectively. The effect that the difference in boron density has on the thermal conductivity of silicon for these samples becomes negligible above 70 K [36, 37], consistent with the previous assumption.

The values presented in figure 6 show a region of values presented for Sample 2, these correspond to the thermal conductivity for a possible range of thickness for the bonds (measured values between $320 \rightarrow 1160$ nm range presented in section 3). However, since the values presented for this sample follow the same shape as samples 1 and 3, the assumption is made for an average thickness of 935 nm, overlapping with the values presented for Sample 3.

The combined errors in the thermal conductivity values are dominated by the uncertainties in the temperature sensor spacing along the samples 2% on the measurement and the uncertainty in the bond thicknesses 4%. The uncertainties for the thermal conductivity of the bond

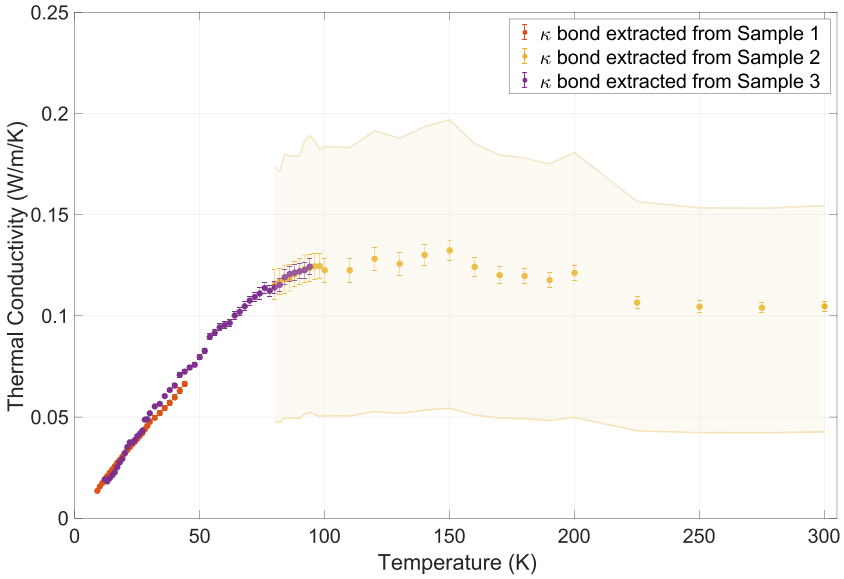

Figure 6. Thermal conductivity curve for hydroxide catalysis bonds extracted using the values from figure 5. The values for Sample 2 are for the possible thickness bond range between 320 nm and 1160 nm with the middle data points fitting a 935 nm bond thickness.

were evaluated by both Monte Carlo analysis and propagation of errors, for each temperature point, and were found to be in approximate agreement for values below 90 K with maximum uncertainty of 26% for an individual sample.

6. Discussion and conclusions

The measured thermal conductivity of hydroxide catalysis bonds between silicon substrates presented here will enable more precise modelling of heat flows in future cryogenic gravitational wave detectors and other relevant experiments. For bonds between sapphire substrates presented by Suzuki *et al* [24], it is possible to calculate the thermal conductivity at 20 K to be $0.0072 \rightarrow 0.012$ $\mathrm{Wm^{-1}K^{-1}}$, assuming a bond thickness of $61 \rightarrow 100$ nm [32]. This is lower than those presented here ($3.20 \pm 0.06 \times 10^{-2}$ $\mathrm{Wm^{-1}K^{-1}}$ at 20 K). However, a direct measurement of the thickness for sapphire bonds is required to accurately compare.

The impact of these results can be assessed in relation to future gravitational wave detectors operating at 20 K such as the cryogenic, low frequency interferometers of the Einstein Telescope (ET-LF) [16]. For ET-LF, it is planned to have 18 kW of laser power circulating in the optical cavities, with the mirror temperatures held at 20 K. Mirror coatings in current and future GW detectors typically aim for optical absorptions no greater than one part-per-million (ppm). The temperature gradient through the planned bond geometry for ET-LF can be calculated for given heat flux, Q, by $\Delta T = QL_{\mathrm{bond}}/A\kappa_{\mathrm{bond}}$, where the other symbols have been defined previously. If there is 1 ppm absorption in the mirrors, the induced temperature gradient across the bond is calculated to be 14.5 μK. If the absorption rises to 20 ppm, then the expected temperature difference across the bonds for a ET-LF prototype would rise to 262.2 μK.

The results presented here only include the hydroxide catalysis bonds at the test mass, and do not include the bonds required at the penultimate mass. Despite this, the results presented do not suggest that the additional bond interfaces would be significant or problematic for the successful operation of cryogenic interferometers.

Therefore the thermal conductivity of hydroxide catalysis bonds are likely to be compatible with all planned cryogenic interferometer configurations. When combined with the extensive demonstration of hydroxide catalysis bonds in the current room temperature gravitational wave detectors, both in terms of reliability and thermal noise performance, the continued use of this technology for cryogenic operation remains attractive.

Moreover, the samples presented here, with multiple bonds, have enabled the first results for the thermal conductivity of the individual silicate bonds from 9 to 300 K. This will allow precise modelling of future interferometers that might require more demanding heat extraction parameters, in addition to being of relevance to other experiments requiring high levels of stability and minimal thermal gradients.

Data availability statement

The data that support the findings of this study are openly available at the following URL/DOI: https://10.5525/gla.researchdata.1472.

Acknowledgments

We are grateful for financial support from STFC (ST/N005422/1, ST/V001736/1 and ST/V005634/1), the International Max Planck Partnership, the Royal Society (DH120021) and the University of Glasgow. We thank our colleagues in the LIGO Scientific Collaboration (LSC), LIGO being a facility operated on behalf of the NSF by Caltech and MIT. We also thank colleagues in the Virgo Collaboration, KAGRA collaboration, the Cosmic Explorer collaboration and the Einstein Telescope collaboration, and within SUPA for their interest in this work. A special thanks to Russell Jones for CAD support and Gerry O'Hare at UWS for technical support. This article has LIGO Document No. LIGO-P2300051.

ORCID iDs

Mariela Masso Reid https://orcid.org/0000-0001-6177-8105
Karen Haughian https://orcid.org/0000-0002-1223-7342
Alan V Cumming https://orcid.org/0000-0003-4096-7542
Giles Hammond https://orcid.org/0000-0002-1414-3622
James Hough https://orcid.org/0000-0003-3242-3123
Anna-Maria van Veggel https://orcid.org/0000-0002-5634-5169
Sheila Rowan https://orcid.org/0000-0002-0666-9907

References

[1] Abbott B P *et al* 2019 GWTC-1: a gravitational-wave transient catalog of compact binary mergers observed by LIGO and Virgo during the first and second observing runs *Phys. Rev.* X **9** 031040
[2] Abbott B P *et al* 2021 GWTC-2: compact binary coalescences observed by LIGO and Virgo during the first half of the third observing run *Phys. Rev.* X **11** 021053
[3] Abbott B P *et al* 2011 GWTC-3: compact binary coalescences observed by LIGO and Virgo during the second part of the third observing run *Phys. Rev.* X submitted

[4] Abbott B P *et al* 2016 GW150914: the advanced LIGO detectors in the era of first discoveries *Phys. Rev. Lett.* **116** 131103
[5] Aasi J *et al* 2015 Advanced LIGO *Class. Quantum Grav.* **32** 074001
[6] Accadia T *et al* 2012 Virgo: a laser interferometer to detect gravitational waves *J. Instrum.* **7** 03012
[7] Grote H (LIGO Scientific Collaboration) 2010 The GEO 600 status *Class. Quantum Grav.* **27** 084003
[8] Barr B W *et al* 2002 Silica research in glasgow *Class. Quantum Grav.* **19** 1655–62
[9] Gwo D *U.S. Patent* No. US 6,284,085 b1
[10] Gwo D Hydroxide-catalysed bonding *U.S. Patent* No. US 6,548,176 b1
[11] Gwo D 1998 Ultraprecision bonding for cryogenic fused-silica optics *Proc. SPIE* **3435** 136–42
[12] Everitt C W F *et al* 2011 Gravity probe B: final results of a space experiment to test general relativity *Phys. Rev. Lett.* **106** 221101
[13] Cagnoli G, Gammaitoni L, Hough J, Kovalik J, McIntosh S, Punturo M and Rowan S 2000 Very high *Q* measurements on a fused silica monolithic pendulum for use in enhanced gravity wave detectors *Phys. Rev. Lett.* **85** 2442–5
[14] Cunningham L *et al* 2010 Re-evaluation of the mechanical loss factor of hydroxide-catalysis bonds and its significance for the next generation of gravitational wave detectors *Phys. Lett.* A **374** 3993–8
[15] Pitkin M, Reid S, Rowan S and Hough J 2011 Gravitational wave detection by interferometry (ground and space) *Living Rev. Relativ.* **14** 5
[16] ET design report update 2020 2020 *European Commission* Report No. ET-0007B-20
[17] Reitze D (LIGO laboratory: California Institute of Technology, LIGO Laboratory: Massachusetts Institute of Technology, LIGO Hanford Observatory and LIGO Livingston Observatory) 2019 The US program in ground-based gravitational wave science: contribution from the LIGO laboratory *Bull. AAS* **51**
[18] Adhikari R X *et al* 2020 A cryogenic silicon interferometer for gravitational-wave detection *Class. Quantum Grav.* **37** 165003
[19] Anderson O L and Bommel H E 1955 Ultrasonic absorption in fused silica at low temperatures and high frequencies *J. Am. Ceram. Soc.* **38** 125–31
[20] Fine M E, Van Duyne H and Kenney N T 1954 Low-temperature internal friction and elasticity effects in vitreous silica *J. Appl. Phys.* **25** 402–5
[21] Marx J W and Sivertsen J M 1953 Temperature dependence of the elastic moduli and internal friction of silica and glass *J. Appl. Phys.* **24** 81–87
[22] McSkimin H J 1953 Measurement of elastic constants at low temperatures by means of ultrasonic waves-data for silicon and germanium single crystals and for fused silica *J. Appl. Phys.* **24** 988–97
[23] Rowan S, Byer R, Fejer M, Route R, Cagnoli G, Crooks D, Hough J, Sneddon P and Winkler W 2003 Test mass materials for a new generation of gravitational wave detectors *Proc. SPIE* **4856** 292–97
[24] Suzuki T *et al* 2006 Application of sapphire bonding for suspension of cryogenic mirrors *J. Phys.: Conf. Ser.* **32** 309
[25] Lorenzini M *et al* 2010 Silicate bonding properties: investigation through thermal conductivity measurements *J. Phys.: Conf. Ser.* **228** 012019
[26] Elliffe E J, Bogenstahl J, Deshpande A, Hough J, Killow C, Reid S, Robertson D, Rowan S, Ward H and Cagnoli G 2005 Hydroxide-catalysis bonding for stable optical systems for space *Class. Quantum Grav.* **22** S257–67
[27] Reid S, Cagnoli G, Elliffe E, Faller J, Hough J, Martin I and Rowan S 2007 Influence of temperature and hydroxide concentration on the settling time of hydroxy-catalysis bonds *Phys. Lett.* A **363** 341–5
[28] Beveridge N L *et al* 2011 Low-temperature strength tests and SEM imaging of hydroxide catalysis bonds in silicon *Class. Quantum Grav.* **28** 085014
[29] Iler R K 1979 *The Chemistry of Silica* (Wiley)
[30] Phelps M, Masso Reid M, Douglas R, van Veggel A A, Mangano V, Haughian K, Jongschaap A, Kelly M, Hough J and Rowan S 2018 Strength of hydroxide catalysis bonds between sapphire, silicon and fused silica as a function of time *Phys. Rev.* D **98** 122003
[31] Deal B E and Grove A S 1965 General relationship for the thermal oxidation of silicon *J. Appl. Phys.* **36** 3770–8

[32] van Veggel A A and Killow C 2014 Hydroxide catalysis bonding for astronomical instruments *Adv. Opt. Technol.* **3** 293–307
[33] White G and Meeson P 2002 *Experimental Techniques in Low-Temperature Physics* (Oxford University Press)
[34] Lees C H 1908 The effects of temperature and pressure on the thermal conductivities of solids. Part II. The effect of low temperatures on the thermal conductivities of pure metals and alloys *Proc. R. Soc.* **80** 143–5/536
[35] Peirce B O and Willson R W 1898 On the thermal conductivities of certain poor conductors. I *Proc. Am. Acad. Arts Sci.* **34** 3–56
[36] Li S S 1978 The dopant density and temperature dependence of hole mobility and resistivity in boron doped silicon *Solid-State Electron.* **21** 1109–17
[37] Asheghi M, Kurabayashi K, Kasnavi R and Goodson K 2002 Thermal conduction in doped single-crystal silicon films *J. Appl. Phys.* **91** 5079–88